TÉCNICO LISBOA

Extended abstract

Laser cladding of new hard coatings for manufacturing and repairing cermet tools

Bernardo José Jorge Diniz

Abstract

The aim of this work was deposit coatings containing an high volume fraction of reinforcement phases, from WC-4Co-5Ni, WC-10Ni e 25NiCr-75CrC powders with laser cladding.

The deposited coating thickness ranges from 1mm to 1.6mm with porosity volume fraction varying, between 3% and 6%. In the WC reinforced coatings, no cracks were observed. In the NiCr – CrC coating there is some degree of cracking, attributed to thermal stresses developed during solidification and cooling of the coating.

In WC – FeCoNi coating, the microstructure is characterized by the presence of faceted WC particles, W_2C particles with irregular morphologies and M_6C carbides with both, faceted/dendritic morphologies and eutectic morphologies. The matrix, is characterized by the presence of, dendritic γ – (FeNiCo) and Fe_6W_7 and eutectics of γ – (FeNiCo) – M_6C and Fe_6W_7 – M_6C.

In WC – FeNi coating, the microstructure is manly composed of faceted WC particles, faceted and elongated W_2C carbides and eutectic M_6C. The matrix, presents itself, in the form of dendritic γ – (Fe, Ni) and interdendritic eutectic of γ – (Fe, Ni) - M_6C.

The microstructure of NiCr – CrC coating is characterized by the presence of faceted, more or less elongated chromium carbides, namely, Cr_3C_2 and Cr_7C_3 surrounded by an eutectic matrix of (Ni,Cr) - Cr_3C_2 /Cr_7C_3.

Regarding coating hardness, it's constant throughout the coatings thickness, with WC – FeNi coating yielding an average hardness of 780$\pm$50 HV1, the WC – FeCoNi coating and average hardness of 980$\pm$43HV1 and the NiCr – CrC coating an average hardness of 1120HV1$\pm$20HV1. The differences in hardness between the coatings were attributed to the carbide phase volume fraction and differences in hardness of the composite matrix.

Regarding friction coefficient, all coatings yield a dynamic friction coefficient between 0,08 and 0,14, with run-in periods between 5-10 min.

The wear coefficient ,for the different coatings, was calculated yielding a value of $2{,}3\times10^{-6}$ $mm^3/(N.m)$ for the WC – FeNi coating, $3{,}92{,}3\times10^{-6}$ $mm^3/(N.m)$ for the WC – FeCoNi coating and $1{,}9\times10^{-5}$ $mm^3/(N.m)$, for NiCr – CrC coating. It was found that average coating hardness doesn't play a role in the composites wear resistance. The wear resistance was found to be determined by the relation between reinforcement particle hardness and counter body hardness, particle volume fraction and particle size.

Key- words: Composite coatings, laser cladding tungsten carbide, chromium carbide, microstructure, wear behavior

1. Introduction

For many industrial applications, such as cutting tools and mining machinery parts, the surface properties of the materials employed are generally of major importance, since cutting tools are usually subjected to harsh wear and corrosion environment. For this reason, nowadays surface engineering is being more and more considered since it offers an effective and economical mean of improving the durability, effectiveness and service life of components subjected to intensive wear and corrosion environments. To accomplish specific surface properties intended for these applications, such as abrasive wear resistance, it's required the use of multiphase materials, usually metal matrix composites reinforced with a dispersion of hard particles. In this group of materials one can include WC reinforced alloys and Cr_2C_3/Cr_7C_3 based alloys.

Although wear resistance doesn't present itself as an intrinsic material property and rather depends on the nature of the tribological system in which the material is employed, understanding the relations between material properties and microstructure and their influence on the behavior of the material in a given tribological system can be essential for designing and selections of materials for any tribological system.

Among the available hard-facing alloys based on tungsten carbides and chromium carbides, the most commonly used binders are usually, Ni-based, Co-based and iron-based binders.

Usually this composites are deposited by thermal spraying processes, although, these processes usually lead to the presence of defects in the coatings such as porosity, microcracks, unmelted particles and low bonding strength at the interface as a result of interfacial mechanical bonding. This leads to a necessity of depositing these kinds of materials with the aid of some high energy beam techniques such as laser cladding.

Among all the reinforcement phases, tungsten carbides present themselves as the most promising to increase wear resistance of substrates, due to their reported hardness greater than 2000 vickers, good wettability by molten metals, low thermal expansion coefficients, around 3.88-5.65 x 10^{-6} K^{-1} and high melting point (>3000K) [1].

Chromium Carbides aren't usually used in laser cladding processes, since this kind of carbides have low melting points, leading to a full dissolution in the melting zone. Cr_3C_2 can e considered for WC substitutions since it has a reported hardness greater than 2200 vickers. Nevertheless, since the melting point of this carbide is easily surpass during laser cladding, on cooling , the formations of Cr_7C_3 as a primary solidification phase can occur, leading to a decrease in hardness of the composite material, since this carbide reported Vickers hardness of around 1700. It has been found by L.Venkatech et al.[2] that decreasing laser power and increasing processing velocities can be correlated with the formation of this low hardness carbide, hindering the performance of the composite material.

Although laser cladding of WC – based alloys, appears has a promising, it presents some limitations regarding particle loading. Tobar et al.[3] as reported that for a WC particle loading greater that 50%wt, it's increasingly harder for material to flow in the melt pool, leading to melt pool instabilities that result in a tooth edge appearance along the clad. The authors attribute this phenomenon to the high melting point of the ceramic particles and their high concentrations, resulting in the formation of a low fluent material in the melt pool. It's also found by xxx that WC content for Ni-based alloys should not exceed 45%vol, otherwise resulting in the formations of large pores and poor bonding[4].

In the presence of small binder fractions 10-20%wt in WC – based alloys, it is usually required an increased energy density, which can induce high substrate dilutions and increased porosity in the coatings. This results are corroborated by J.Przybylowicz et al.[5] and Mohammad Erfanmanesh et al.[6] findings.

Not much research has been conducted in laser cladding of highly loaded MMC (Metal Matrix Composites) materials, since they present them self has very difficult alloys to deposit under normal processing conditions.

Huang et al. [4] has investigated the wear behavior of laser cladded WC/Ni alloys deposited on H13 steel substrates, reporting an increase of wear resistance by a factor of 5-10 when compared to the H13 tool steel substrate. J.S.Xu et al.[7] tried to establish a relation between particle loading and wear behavior of WC – Ni based alloys, by varying the WC content between of 0-80%wt, reporting the best wear resistance behavior for the alloy with 40%wt in WC. Van Acker et al.[8] investigated the particle size and distribution on wear behavior of WC-Ni based alloys deposited by laser cladding, reporting that in dry sliding conditions, wear resistance increases with increase particle concentration and decrease in particle size. For three-body abrasion, the authors reported that if the abrading particle size is inferior to the size of the reinforcement particles the wear behavior of the composite is manly controlled by the matrix characteristics. Nevertheless, this results have been contradicted by the Xin Tong et al.[9] studies, in which, the authors study the effects on wear behavior of WC particle size, failing to find a clear correlation between these factors.

The aim of this work was to deposit highly loaded MMC coatings on steel substrates, from precursor powders of WC – 10Ni, WC – 4Co – 5Ni and 25NiCr – 75CrC(80%Cr_3C_2 – 20% Cr_7C_3) by means of laser cladding. The resulting coatings where characterized in function of their defects and general characteristics, microstructure evolution during solidification, mechanical properties (surface hardness) and tribological behavior.

2. Experimental

2.1. Materials and methods

In this study, the starting powders, WOKA 7305 (25%NiCr – 75CrC) with a chemical composition of 17.5-22.5%wt Ni, 9.0-10.2%wt C and Cr balanced with nominal particle sizes ranging from 15-45 µm and WOKA 3302 (WC – 10%Ni) with a chemical composition of 8.5-11.5%wt Ni, 5.2-6.0%wt C and W balanced with nominal particle sizes ranging from 15-45 µm. The powders were acquired by TE&M and send to IST where they were characterized by size, composition and element distribution via SEM microscopy (Hitachi S-2400), EDS measurements (Brucker nano XFlash detector 5010) and XRD diffraction using a Philips PW 3710 mpd control with a CuKα1 lamp (λ = 0,15065nm) between 10 and 100º, with a 0,1º step and scanning time of 5s. To confirm their composition.

It was also characterized and used a powder sent by TE&M with commercial reference WOKA 3202 (WC – 17%Co). Some discrepancies were identified in the composition of WOKA 3202 powder. The analyzed powder has shown a real composition of approximately WC – 5%Ni – 4%Co, the powder is clearly composed of Ni rich particles and Co rich particles as showed by the composition map in Figure 1 (b).

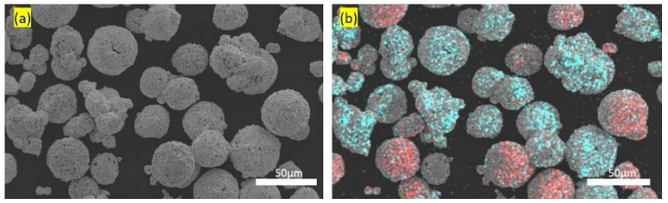

Figure 1 - WC - 5Ni-4Co powder. (a) morphology of the powder (b) EDS map of the powder, blue particles are ni-rich particles and red particles are co-rich particles

It's worth noticing that for all the powders the powder particles are already composite materials composed of reinforcement phase and binder phase.

The individual coatings were then prepared by blown powder laser cladding method, with use of 1,5Kw top-hat diode laser and a computer-controlled XY. The substrates used for the cladding process of the WC-based powders were plates of commercial ck45 steel and for the CrC based powders, plates of commercial 303 stainless steel. Three process parameters were chosen as key operational processing parameters: laser power, scanning speed and powder feed rate. For all coatings the processes parameters were varied to find the best operational conditions for this set-up. Laser power was changed from 500W to 1500W with constant increments of 50W, scanning speed was changed with successive increments of 0,2mm/s from 3mm/s to 14mm/s and powder feed rate was varied from 0.1g/s to 0.35 g/s. The best operational conditions are summarized in table 1.

Table 1 - Parameters used for the laser cladding of individual powders.

Powder	Laser Power (W)	Scanning speed (mm/s)	Powder feed rate (g/s)	Overlap (%)
WC – 10Ni	1100	4	0,17	63
WC – 5Ni-4Co	1350	14	0,3	50
25NiCr – 75CrC	800	10	0,15	53

The beam diameter was kept constant for all samples deposited with a value of 3mm. Argon was used as a shielding gas with flow rate kept constant at 3L/min.

To avoid intense thermal gradients, the substrates were pre-heated at 350ºC. The precursor powders were also pre-heated at 90ºC for 12h, to dry the powders and remove adsorbed water.

2.2. Microstructure characterization

Microstructure characterization was carried out by optical microscopy (Nikon optical magnifier SMZ800 coupled with a Nikon digital sigth Ds-Fi1 camera), scanning electron microscopy (FEG-SEM JEOL JSM-70001F coupled with an Oxford EDS system (INCA Penta Fet x3) and X-ray diffraction Philips PW 3710 mpd control with a CuKα1 lamp (λ = 0,15065nm) between 25 and 75º, with a 0,05º step and scanning time of 2,5s.

Microstructure analysis were carried in transverse cross-section and polished with SiC graded sandpaper in the following order 80, 120, 240, 600, 800, 1000, 2400 and 4800, then polish with diamond paste of 3 and 1 µm and finally with an SiO_2 colloidal suspension.

2.3. Hardness measurements

The hardness of the coatings was evaluated by microhardness tests carried out in under a load of 10N, using a Vickers indenter.

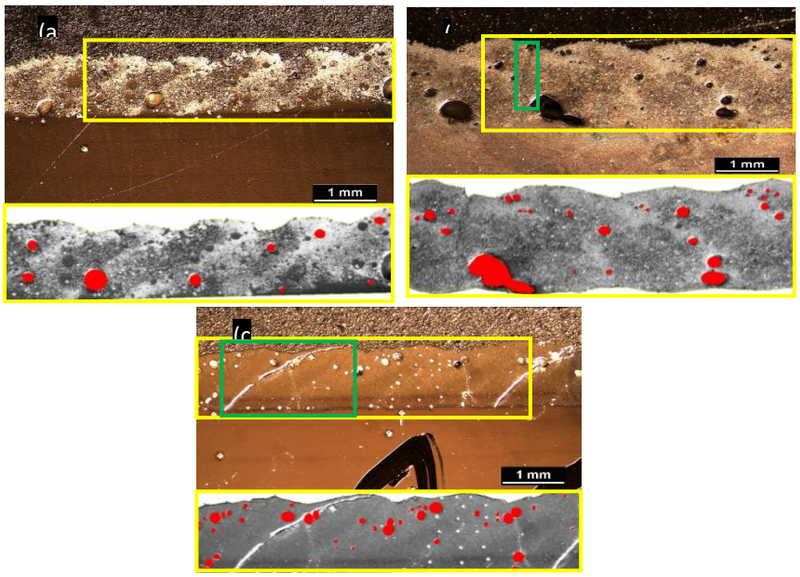

Figure 2 - Transverse cross-sections of the different coatings made from the following precursor powders (a) WC - 4Co - 5Ni; (b) WC - 10Ni; (c) 25NiCr-CrC; In red it can be observed the pore fraction for each yellow marked area and in green its highlighted crack zones

2.4. Wear tests

Dry sliding wear tests were performed using a ball cratering apparatus similar to the one describe by Colaço et al.[10], on samples cut parallel to the coating/substrate interface polished in the same way described for the microstructure transverse cross sections. The counter body used was a 25 mm diameter alumina sphere, which rotates against the sample. The tests were performed at constant sliding speed of 130mm/s, for a sliding distance of 2500m under a normal load of 3N, The wear coefficient was calculated from the volume of removed material determined by measuring the crater area and establishing an equivalent diameter. The wear mechanisms were investigated by SEM observations carried out in SEM Hitachi S-2400 and EDS analysis carried out by a Brucker nano XFlash detector 5010.

3. Results and Discussion

3.1. General coating considerations

3.1.1. Coating characteristics and defects

Three parameters where selected as the main coating characterization variables, coating thickness, porosity fraction, the presence of cracks and coating homogeneity.

The results of this analysis are showed in Figure 2 and summarized in Table 2.

Table 2 – General coating characteristics for the different deposited coatings

Powder reference	Coating height (mm)	Characteristics
WC – 4Co – 5Ni	1.0 ± 0.1	Approx. porosity fraction of 3%; Absence of cracks; Heterogeneous coating microstructure
WOKA 3302	1.6 ± 0.2	Approx. porosity fraction of 6%; Cracks initiate at porosity interfaces and do not propagate though all the coating thickness; Homogeneous coating microstructure
WOKA 7305	1.1 ± 0.1	Approx. porosity fraction of 4%; Cracking from thermal stresses Homogeneous coating microstructure

Considering the results obtained, it's important to try to establish a relation between these characteristics and laser processing conditions. Two major variables emerge by combining process conditions showed in Table 1, power density and interaction time. Power density is obtained by the ration between power used and the laser beam area and the interaction time is obtained by dividing the laser beam diameter by the laser scanning speed.

For each coating, these variables are summarized in table 3.

Table 3 - Power densities and interaction time for each coating deposited

Powder reference	Power Density (W/mm^2)	Interaction time (s)
WC – 4Co – 5Ni	191	0.21
WOKA 3302	156	0.75
WOKA 7305	113	0.30

In Figure 3, one can observe the differences regarding coating homogeneity. Both coatings deposited from WC – 10Ni and 25NiCr – 75CrC powders are relatively homogeneous.

A clear distinction can be seen for the coating deposited from WC – 4Co – 5Ni. In this coating one can be observed the presence of zones absent of WC particles.

The predominant mechanism for homogeneity in laser cladding processes is the intensity of the convection currents generated in the melt pool. In order to study the impact of the connection currents generated in the melt pool, for each coating one can use the model proposed by C.Chan et al.[11], rearranged in order to explicitly introduce power density and interaction time, as variables, such as:

$$S = \frac{\sigma' q d}{\eta V_f k} = \varphi_m I_{abs} \tau \qquad (1)$$

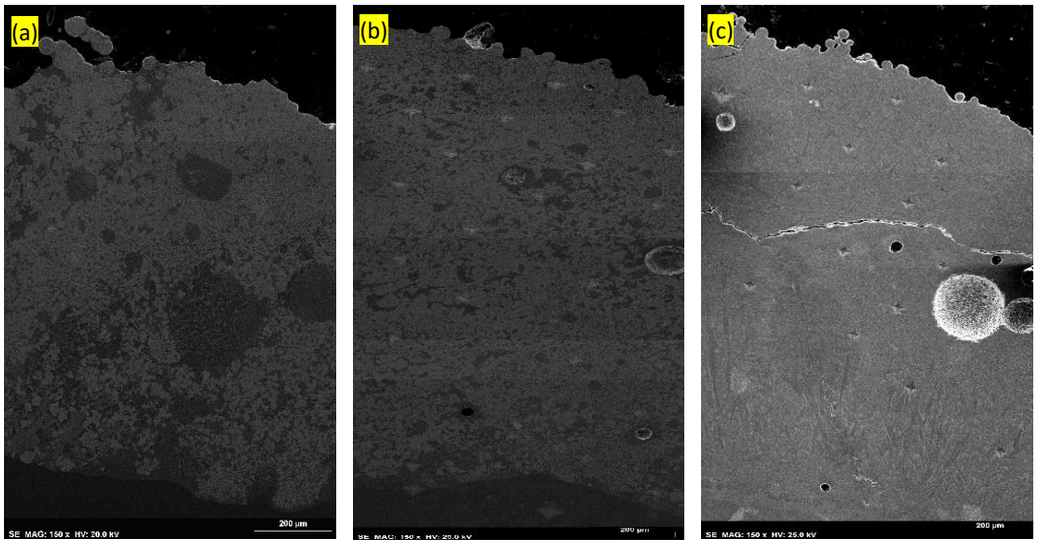

Figure 3 - SEM imagens of the coatings microstructures at low magnification (x150); (a) WC - 4Co - 5Ni; (b) WOKA 3302; (c) WOKA 7305

Where φ_m is a material dependent constant that relates the surface tension changes with temperature, the viscosity and the material thermal conductivity, considered equal for both materials, I_{abs} is the absorbed irradiance or power density and τ is the interaction time.

Considering this, it's clear that for WC – 10Ni coating, convection processes should be of more importance than for WC – 4Co – 5Ni coating, however, since this systems are expected to have viscosities that hinder material flow, due to the presence of high volume fractions of solid WC particles, the material constant can be assumed to have a minor importance. So, the S number for WC – 10 Ni coating is about 130 and for WC -4Co -5Ni about 30. Both values present itself as low values, leading to the conclusion that, although convective movements should play an important role in coating homogeneity, for highly loaded WC composite coatings, another homogeneity mechanisms should be present.

To further understand the interaction between reinforcement particles and liquid in the molten metal, it's necessary to first estimate the temperature distribution.

Additionally, the diffusion profile for C and W atoms, was establishes as a function of particles distance, for the WC reinforced coatings.

3.1.2.Temperature distribution Estimations.

The temperature distribution in the melt pool was calculated using Ashby's and Easterling model [12]. The authors show that the melt pool temperature profile can be analytically approximated by the following equation:

$$T(z,t) = T_0 + \left(\frac{AP_f}{2\pi k}\right)\frac{1}{V_f\sqrt{t(t+t_0)}}e^{-\frac{(z+z_0)^2}{4\alpha_T t}} \qquad (2)$$

Where T is the temperature, z is the height of the clad, t is the time, A is the absorptivity ,P_f is the laser power, k it's the material thermal conductivity, α_T is the thermal diffusivity, V_f is the scanning speed, T_0 is the substrate initial temperature and t_0 is the time that takes heat to travel the half of the laser beam diameter r_0 and it's equal to $t_0 = \frac{{r_0}^2}{4\,\alpha_T}$.

It's important to consider that this is a simple model that doesn't take into consideration changes in temperature caused by phase transformations and fusion enthalpies.

To feed the model it was necessary to estimate some properties and make some approximations, namely, thermal conductivity of the composite material. The thermal conductivities for all coatings were obtained by the Maxwell-Garnett equation (3), which as proven to be a better approximation for thermal conductivity of MMC than a simple mixture law[13].

$$k_{eff} = k_1\left(\frac{k_2(1+2V_2) - k_1(2V_2-2)}{k_1(2+V_2) - k_2(1-V_2)}\right) \qquad (3)$$

Where, k_1 is the thermal conductivity of the binder phase, $k_2$the thermal conductivity of the reinforcement particles and V_2 the volume fraction of the reinforcement particles, the values of V1 and V2 were obtained by image analysis of figure 3, and are represented in figure 4.

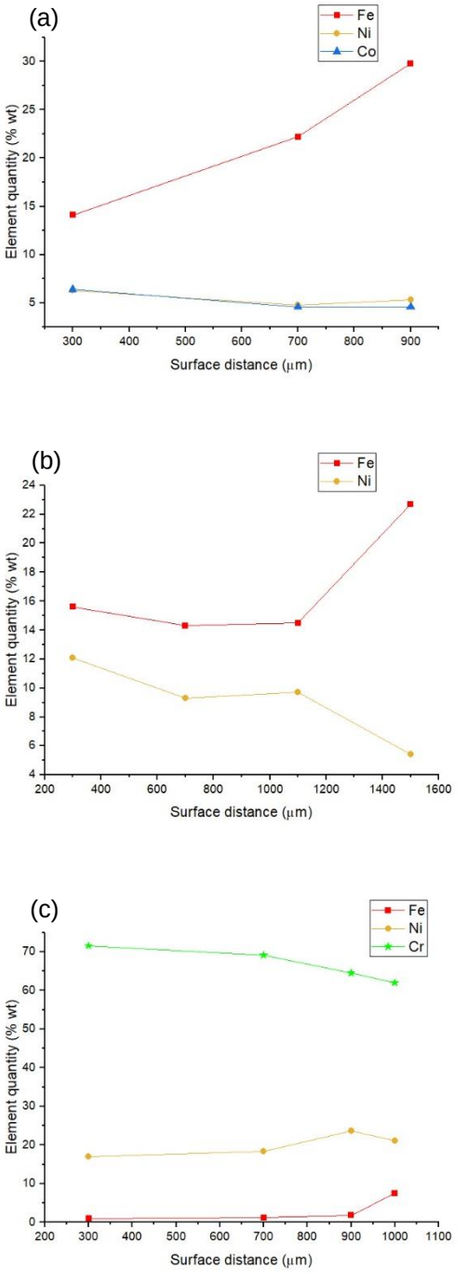

Figure 4 - Element variation as a function of surface distance for (a) WC - 4Co-5Ni (b) WOKA 3302 (c) WOKA 7305

To estimate the composite thermal properties, it was also needed to estimate binder conductivity. This was made by the application of the mixture law and the volume fractions of reinforcement particles in the coatings. These estimations were made by image analysis of Figure 3 and the percentage of each element estimated by EDS. These variables are summarized in table 4.

Table 4 - Thermal conductivity of the different constituents of the composite coatings and the volume fraction of reinforcement and binder phase

	WC - FeCoNi			
	Fe	**Ni**	**Co**	**WC**
Thermal conductivity ($Wm^{-1}K^{-1}$)	35 [14]	55 [63]	35 [63]	57 [15]
Volume fraction in coatings	$\sum Fe + Ni + Co = 36{,}5\% \pm 13$			63,5 %±13

	WC - FeNi			
	Fe	**Ni**	**Co**	**WC**
Condutividade térmica ($Wm^{-1}K^{-1}$)	35 [14]	55 [63]	-	57 [15]
Percentagem no revestimento	$\sum Fe + Ni = 28$ %±12		-	72%±12

	NiCr - CrC	
	NiCr	**CrC**
Condutividade térmica ($Wm^{-1}K^{-1}$)	35 [14]	35 [14]
Percentagem no revestimento	$\sum Fe + Ni = 25$ %	$\sum Fe + Ni = 75$ %

This allowed the estimation of thermal conductivity to be used as an input for the temperature model.

In table 5 one can find the inputs fed to Ashby's model.

Table 5 - Input variables and respective values for each MMC

	WC - FeCoNi	WC - FeNi	NiCr - CrC	Unidades
Raio do feixe laser (r_0)		0,0015		m
Potência do feixe laser (P_f)	1350	1100	800	W
Velocidade relativa do feixe laser (V_f)	0,014	0,004	0,01	ms^{-1}
Temperatura inicial do substrato (T_0)		350		ºC
Temperatura de fusão do ligante majorada (T_1)	1538 [16], [17]		1425 [18]	ºC
Profundidade do revestimento (z)	0,0011	0,0017	0,0012	M
Condutividade térmica do compósito estimada	49,74	52,72	25 [19]	$Wm^{-1}K^{-1}$
Difusividade térmica do compósito estimada	$15x10^{-6}$ [15]		$6x10^{\wedge-5}$ [66]	m^2s^{-1}
Absortividade calculada pela eq. (28)	42,7	33,7	10,5	%

The thermal profiles obtained can be observed in Figure 5. The maximum surface temperature occurs for WC – FeNi coating being approximately 2935ºC as for WC – FeCoNi coating the surface temperature takes a value of 2859ºC. Since the melting temperature listed for WC particles is 2870 ºC. For the NiCr-CrC alloy, it's worth noticing that the estimated surface temperature peaks at around 2418ºC, which is much higher than the carbide melting temperature (Cr_7C_3 ~ 1766ºC and Cr_3C_2 ~ 1811ºC), leading to the formation of an entirely liquid melt pool, as opposed to the WC coatings, where it's expected the formation of a solid enriched melt pool.

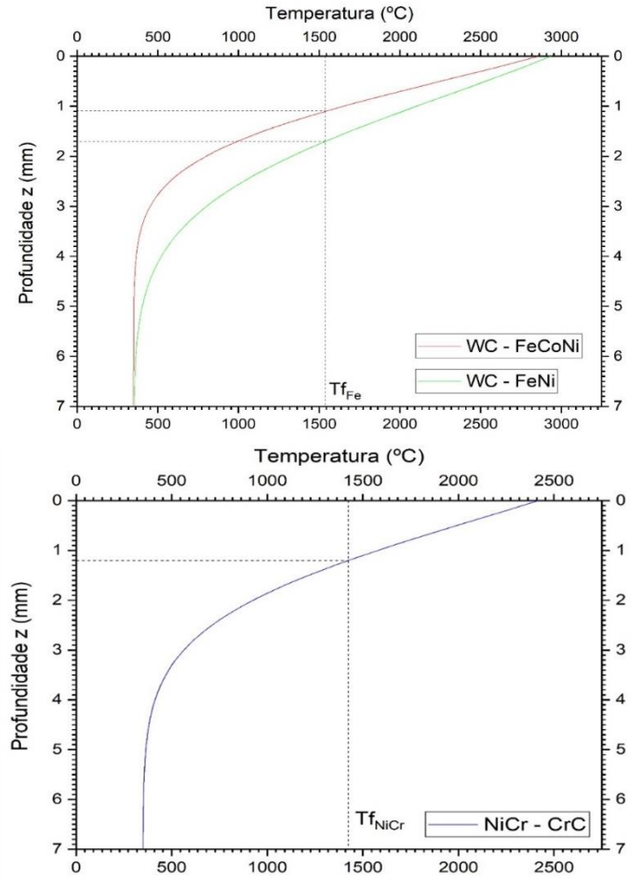

Figure 5 - Temperature profile obtain according to the input data from table 5 and Ashby and Easterling model

To understand what happens to the solid WC particles in the melt pool, as a functions of deposition para meters, the concentration profile for both W and C, as a function of particles distance, was calculated using a solution of Fick's second Law.

$$\frac{C_0 - C_x}{C_0 - C_0} = erf\left(\frac{x}{2\sqrt{D\tau}}\right) \quad (5)$$

Where, D is the diffusion coefficient that a solute atom has in a Fe melt pool and τ is the interaction time

Since the molten pool should manly be composed of iron, as expected from coating element distribution presented in figure 4, and, since both Ni and Co are substitutional atoms of iron, one can assume that the diffusion coefficients of W and C in the melt pool, can be well approximated by the diffusion coefficients of W and C in

liquid iron. The diffusion coefficients for both W and C in liquid iron are presented in table 6.

The diffusion profiles of the different solute atoms were calculated for a sub-surface coating layer situated at half the thickness values. The melt pool temperatures found in the previously mentioned zones are 2186ºC for WC – FeCoNi coating and 2271ºC for WC – FeNi coating.

In figure 6, it can be seen concentration of the solute atoms, C and W, as a function of particle distance, for the different coatings.

Table 6 - Diffusion coefficients for the different solute atoms at different temperatures

Coatings	Difusion elements	D ($x10^{-2}$ $mm2s^{-1}$)	References
WC - FeCoNi	W	0,66	[56], [57]
	C	0,74	[58],[59], [60], [61]
WC - FeNi	W	0,73	[56], [57]
	C	0,79	[58],[59], [60], [61]

By observation of figure 6, it's expected that the greater particle dissolution should occur for the WC – NiFe coating, leading to the formation of more free carbon atoms, that can diffuse for greater distances, increasing the possibility of porosity formation, by the combination of C with O atoms/molecules, leading to the formation of CO or CO_2 according to:

(1) WC + Energy → W + C

(2) $C + O_2(g) \rightarrow CO_2(g)$ and/or $2C + O_2 \rightarrow 2CO(g)$

When a gas bubble forms, the only way it has to escape the coating is by ascension to the surface, this is not expect to occur with ease in this coatings due too the possibility of high melt pool viscosity, that opposes the bubble movement, that combined with the fact that laser processes yield high solidification velocities leas to the entrapment of the gas bubbles.

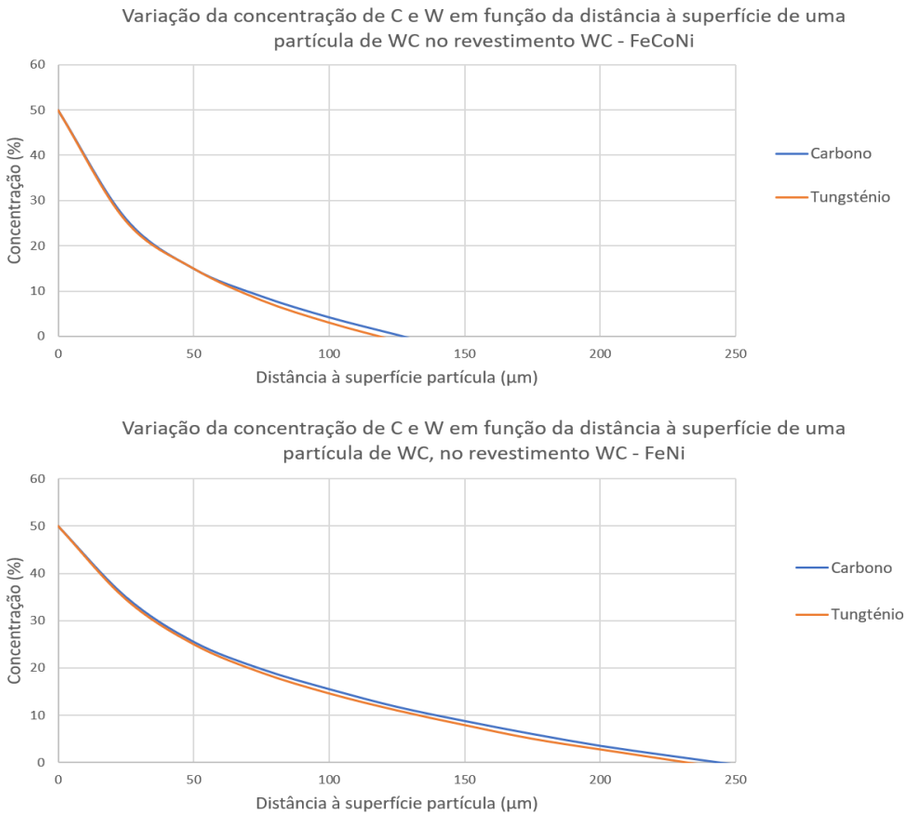

Figure 6 - Concentration profile for W and C atoms in a liquid iron melt pool, for the diferent coatings

3.2. Microstructure and chemical characterization

WC reinforced coatings

The different phases of the coatings were identified by the X-ray diffraction, Figure 9. The results are present in Figure 7. EDS results and SEM images were also used to identify phase chemical composition and morphology.

As seen in Figure 7, the WC - FeCoNi microstructure is manly constituted of unmelted, faceted WC particles, WC secondary precipitates, such as M2C, with irregular morphologies and M6C, with dendritic/faceted morphologies and in the form of interdendritic eutectic, namely, W_2C and Fe_3W_3C. Regarding the matrix, it was identified the presence of dendritic γ – (Fe,Co,Ni) and Fe_6W_7 and the eutectic regions of γ – (Fe,Co,Ni) -M_6C and Fe_6W_7 – M_6C.

The presence of W_2C and M_6C is attributed to the dilution of the WC unmelted particles.

The formation of the different M_6C morphologies was attributed to the coating heterogeneity, leading to the formation of zones od liquid in the hipo and hyper eutectic composition. If the liquid as a hypereutetic composition, de M_6C carbides will solidify as dendriti/faceted carbides, rejecting Fe, Ni and Co to the remaining liquid, pushing the composition to the hipoeutetic compositions, solidifying γ – (Fe,Co,Ni), rejecting W and C to the interdendritic space, if the liquid composition as a carbon weight fraction below 0,015, and a W weight fraction between 0,3 and 0,4, then the liquid can solidify as Fe_6W_7, that by rejecting C to the remaining liquid, can solidify as Fe_6W_7 – M_6C eutectic. If after the initial solidification of the γ – (Fe,Co,Ni), the liquid does not enter the solidification composition of Fe_6W_7, then the remaining liquid solidifies as a interdendritic eutectic of of γ – (Fe,Co,Ni) -M_6C.

The microstructure of WC – FeNi coating, similar to the WC – FeCoNi, is manly constituted of WC unmelted, faceted, WC particles, faceted and elongated W_2C carbides, surrounded by a dendritic γ – (Fe,Ni) solid solution and interdendrític M_6C carbides.

The formation of different morphologies of W_2C was attributed to the fact that, W_2C can solidify with different morphologies according to the solidification of different allotropic phases. Depending on the temperature of the melt pool, the W_2C carbides can appear under bar-like morphology or with irregular shapes as found by Q.Li et al. [30]. The bar-like morphology is attributed to the formation of the allotropic high temperature phase B- W_2C, and the formation of irregular W_2C precipitates is attributed to the solidification of the intermediate allotropic phase B’ – W_2C.

It’s also found that, WC particles in WC – FeNi coating present themselves with 4x the size of the WC – particles in WC – FeCoNi coating. This is attributed to the differences in interaction time. Particle growth is a multi-mode processes controlled by diffusion controlled 2D – abnormal grain growth and nucleation, and by the tendency that a composite has to minimize is internal energy, by merging WC particles (coalescence). Both these processes are more facilitate in WC – FeNi coating, due to higher power densities and lower interaction times.

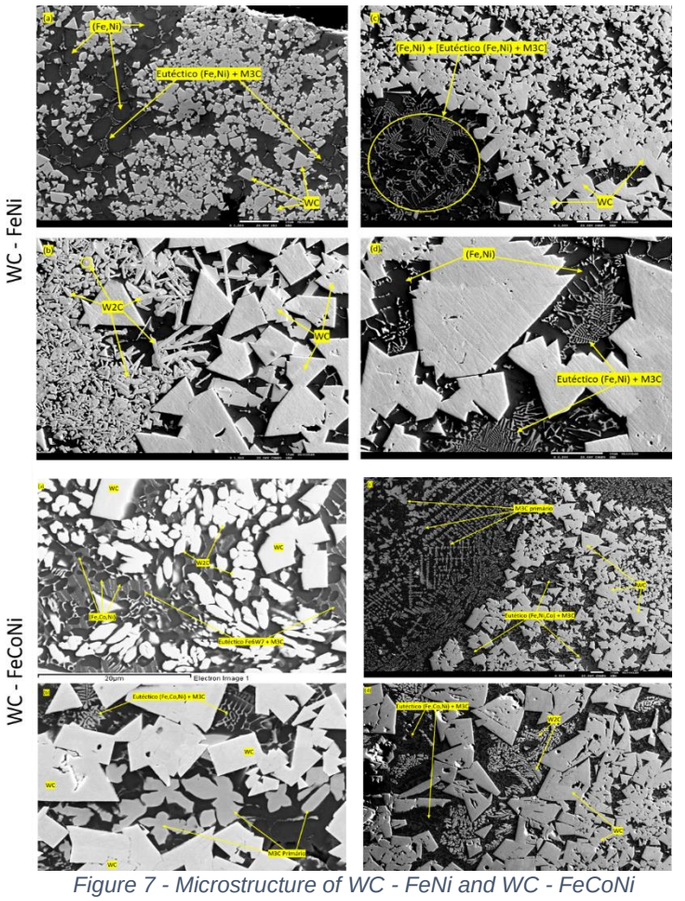

Figure 7 - Microstructure of WC - FeNi and WC - FeCoNi coatings

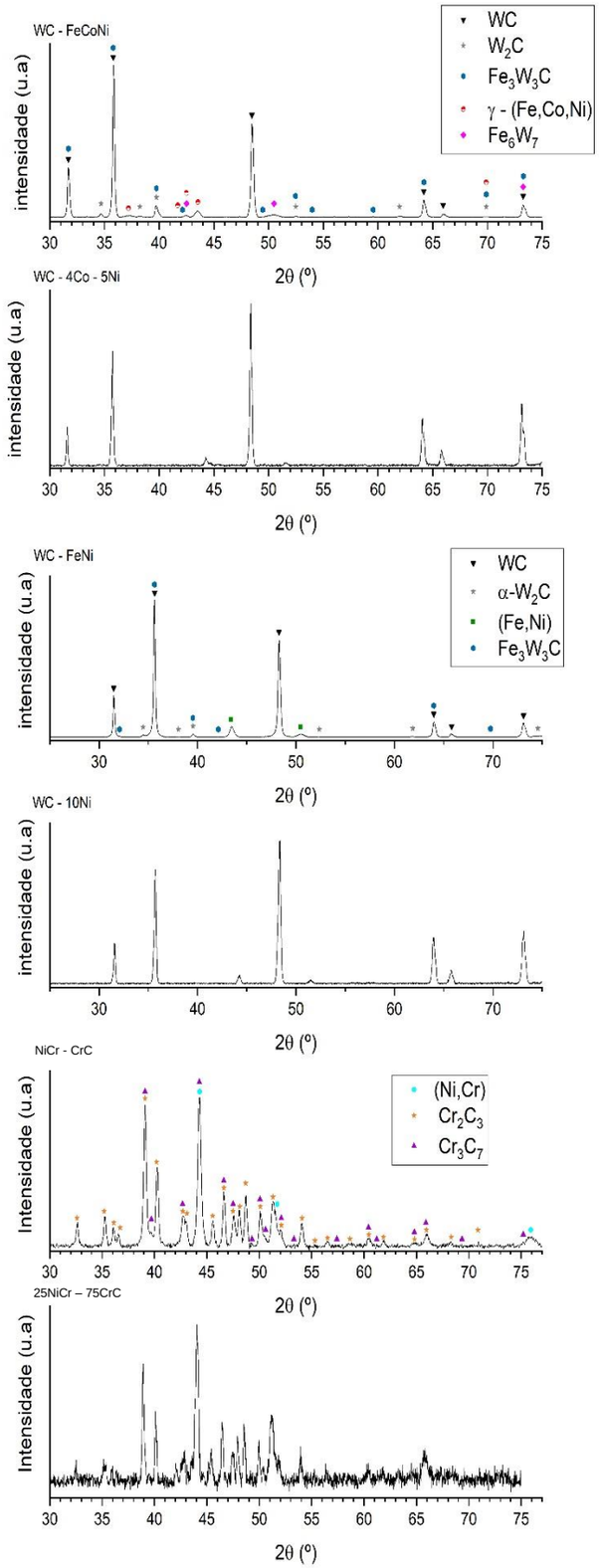

Figure 9 - XRD patterns for the respective deposited coatings and precursor powders

NiCr – CrC coatings

The phases present in the microstructure were identified by XRD in Figure 9. As seen in Figure 7, the microstructure is composed of three main phases, two chromium carbides, Cr_3C_2 and Cr_7C_3 and a Ni-rich solid solution (Ni-Cr) eutectic matrix of (Ni,Cr) - Cr_3C_2/ Cr_7C_3 eutetic . The solidification of the coatings starts with the precipitation of Cr_7C_3 at around 1650ºC, since this is the first phase to form, it grows freely, solidifying as elongated and faceted precipitates. As these carbides solidify and the melt pool cools down, the liquid enters in the formation zone of Cr_3C_2 carbide, that can nucleate and grow by heterogeneous nucleation on the previously formed carbides. The solidification process os these carbides leads the enrichment of the remaining liquid with Ni, pushing the liquid composition towards the eutectic region, solidifying as (Ni,Cr) - Cr_7C_3 - Cr_3C_2 eutectic at a temperature of 1255ºC.

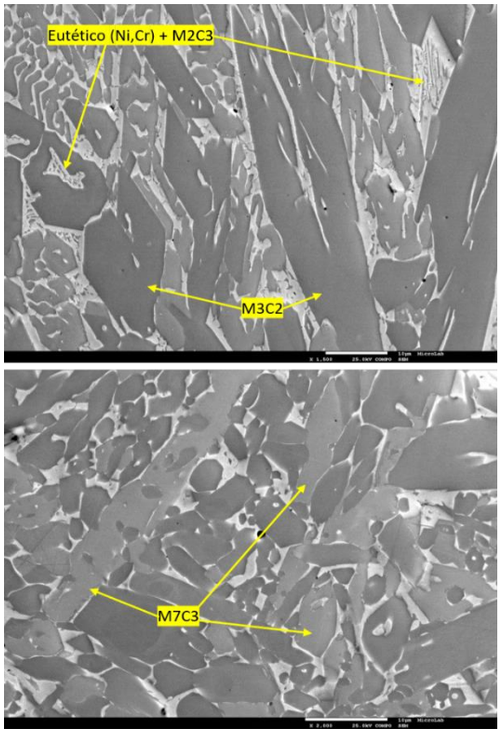

Figure 8 - Microstructure of the NiCr - CrC coating

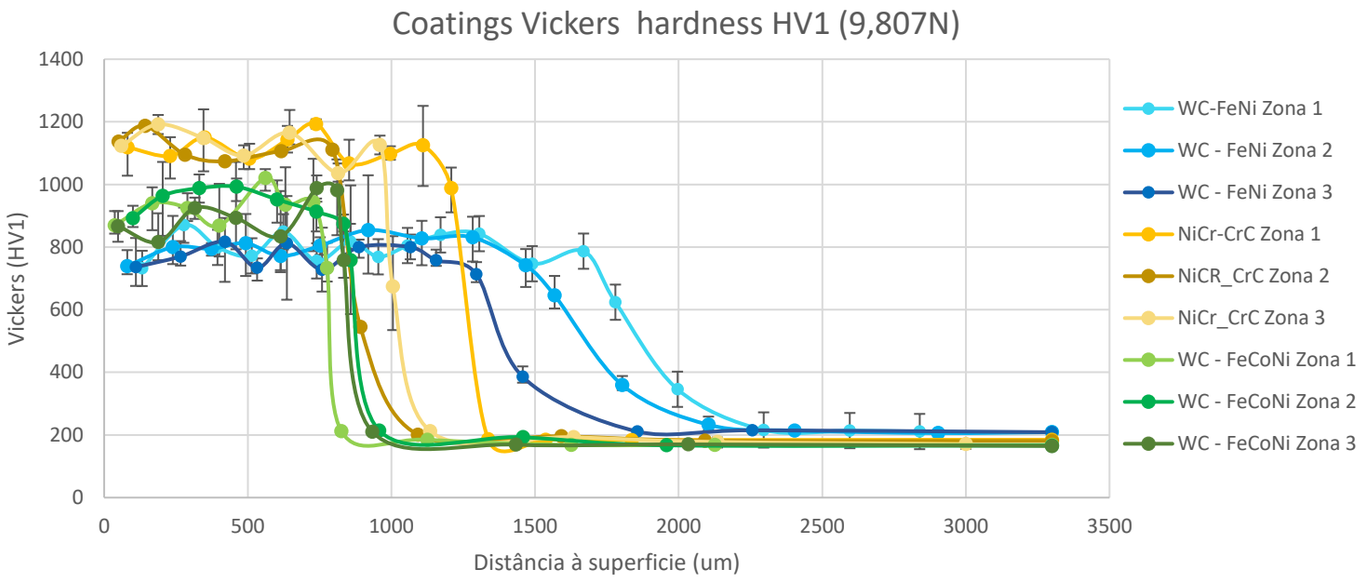

Figure 10 - Microhardness in-depth profile made in three different zones in the transverse cross-sections of the different coatings

3.3. Hardness and wear test

The microhardness profiles in the transverse cross-sections of the coatings are present in Figure 10.

As seen, the hardness values for the different coatings don't present drastic changes with depth, with coating hardness remaining more or less constant with average values of 780HV1 for WC – FeNi, 920 HV1 for WC – FeCoNi and 1120 HV1 for NiCr – CrC. The wear coefficient for the different coatings, is present in Figure 10.

This is attributed to the presence of a higher carbide fraction in NiCr – CrC coating. Cr_7C_3 has a reported hardness value of around 1856HV11 and Cr_3C_2 of around 2121 HV10 [31]. The greater hardness of WC – FeCoNi coating is manly attributed to the presence of a harder matrix, mainly due to the presence of dendritic/faceted M_6C carbides.

By comparing the composite average hardness and wear coefficients, it's obvious that, for this kind of coatings, the wear coefficients is not proportional to the average composite hardness, since the coatings with lower hardness values, are the ones with higher wear coefficient. This is not uncommon in MMC as described by Colaço et al.[10] In this study, the authors found that for MMC, wear rate is independent of the average composite hardness, and rather depends on the hardness of the reinforced particles in relation to counter-body hardness, their size and their volume fraction. In Figure 12, 13 and 14 are present the worn surfaces micrographs for the different coatings.

The NiCr-CrC coating shows signs of slight abrasion as a result of de detachment of small particles from the alumina counter-body, that lead to the formation of grooves on the wear surface. This coating also shows the formations of a tribological layer, rich in oxides, that, when removed, can led to the formation of wear debris that can accumulate in the borders of the interface, or inside coating porosity. In some cases, it can also be seen cracks and detachment of coating material.

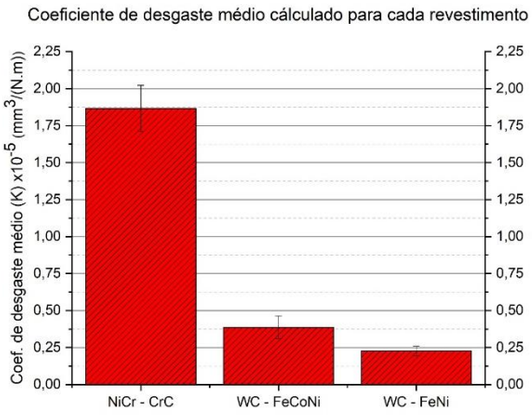

Figure 11 - Abrasive wear volume and rate for the different coatings

Regarding WC reinforced coatings, the wear craters appear shallower, with less signs of abrasion. The small grooves appear to be caused by small alumina particles acting as free bodies during the abrasion test. The formations of a tribolayer it's also seen. This layer usually appears filling up cavities between WC particles, and it's detachment can lead to the formation of wear debris. For WC – FeNi coating, it's noticeable the presence of big alumina particles, as the result of counter-body deterioration.

It's worth noticing that, although the presence of dendritic/faceted M_6C type carbides in WC – FeCoNi coating, increases de composite average hardness, when compared to the WC – FeNi coating, this carbides are not hard enough to sustain the indentation and grooving of the counter body asperities, as seen in figure 12. So the presence of this carbides hinder wear resistance of the composites, since they hinder the tenacity of the matrix, leading to a faster embrittlement of the matrix due to plastic deformation that can result in aggravated loss of material, also, the embrittlement of the matrix can lead to the propagation of cracks through the composite resulting in large volumes of material removed.

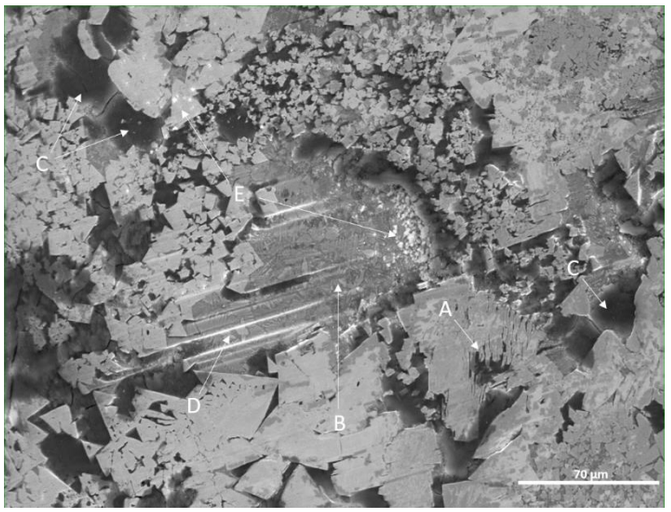

Figure 12 - Worn surface micrograph of WC - FeCoNi coating

The abrasion mechanism observed are correlated with the formation of small alumina particles. The formation of this particles can result of the degradation of the counter-body due to the contact pressures surpassing the rupture modulus of the counter-body, leading to the formation of small particles or they can be formed by the faceted carbides indentation in a counter-body surface defect, leading to stress concentration that can result in the detachment of counter body particles. In order to estimate the contact pressures developed during the wear tests, the Hert'z model for elastic contact [34] was applied, since both counter-body and coatings are manly ceramic materials. The material properties used to feed the model were, for WC - FeCoNi coating it was estimated a Young modulus of 499 GPa and a Poisson coefficient of 0,258, for WC – FeNi a young modulus of 538 GPa and a Poisson coefficient of 0,254 and for NiCr – CrC coating a young modulus of 124 GPa and a Poisson ratio of 0,3[35]. This yield and estimated maximum contact pressure of 567 Mpa for WC – FeCoNi, 578 MPa for WC - FeNi and 332 MPa for NiCr – CrC. In addition, the material yield stress was estimated. For WC – FeCoNi to be 387 MPa, for WC – FeNi 395 MPa and 226Mpa and for NiCr – CrC coating. It's worth noticing that in the wear test conditions, the estimated yield stress of the composite materials wasn't reached by the mean contact pressures.

Nevertheless, it's worth noticing that the mean contact pressures (2/3 of Pmax) doesn't reach the rupture modulus of alumina or the yielding value for the coating. In this case, the formation of alumina debris, should be through the detachment process resulting from a hard faceted carbide identing in a counter-body surfeca defect.

It's worth noticing that, when the counter-body starts showing degradation, with material detachment, the wear dynamic changes, since the contact will now be established between coating and the small alumina particles, leading to an increase in the contact pressures, due to the contact area reduction.

.

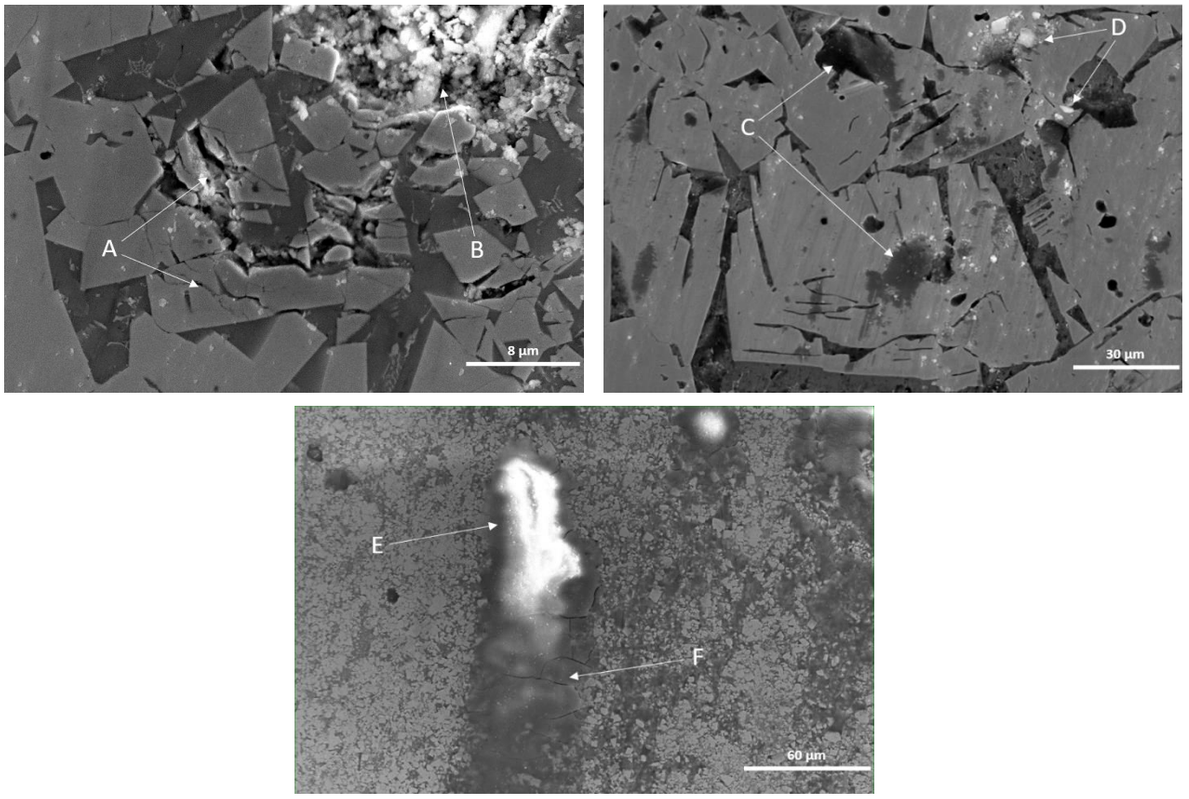

Figure 13 - Worn surface micrograph of WC - FeNi coating

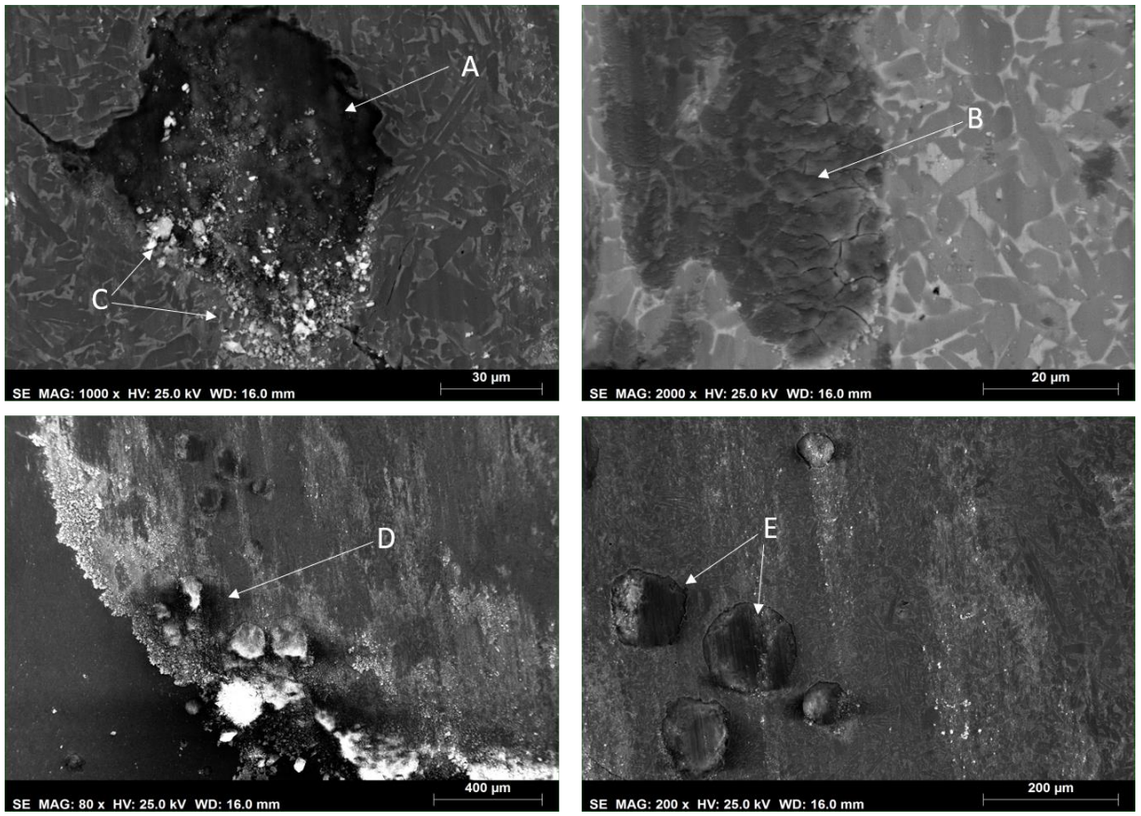

Figure 14 - Worn surface micrograph of NiCr - CrC coating

4. Conclusions

The coatings were study regarding coating general characteristics, microstructure, hardness and wear behavior. Some interesting results are given bellow:

(1) All powders were able to be deposited onto steel substrates;

(2) In WC coatings, substrate dilution wasn't avoided.

(3) Cracking of WC coatings can be avoided by controlling processing parameters. The same was not found for the NiCr – CrC coating, where cracking was attributed to the formation of elongated and faceted chromium carbides.

(4) For WC coatings, coating homogenization was found to be controlled by diffusion processes in the melt pool, depending manly on the interaction time. For the NiCr – CrC, coating no homogenization problems were observed since all precursor powders melt during coating deposition.

(5) The WC coating microstructures depend on the level of homogenization of the coating. When the homogenization leads to significant differences in chemical composition throughout the coating, the formation of M6C carbides can be of primary dendritic/faceted rather than the expected interdendritic eutectic in homogeneous coatings, also, this differences can lead to the formation off Fe_6W_7 phase in the microstructure as described previously.

(6) The NiCr – CrC coating solidifies following the phase diagram, without the formation of unexpected phases. The formation of elongated and faceted primary carbide phases can lead to the formation of cracks.

(7) The wear behavior of the coating is not depend on the respective average coating hardness, rather, it depends on the relation of hardness between reinforcement particles and counter-body, volume fraction of reinforcement phases, their size and distribution.

(8) The wear coefficient appears very promising, with WC – FeNi yielding the lowest value of $1{,}4x10^{-10}$ mm^3/Nm, followed by WC – FeCoNi with $2{,}3x10^{-10}$ mm^3/Nm and NiCr – CrC yielding a value of $1{,}2x10^{-9}$ mm^3/Nm.

(9) The wear mechanisms are manly, fragmentation of WC and counter-body particles, that can lead to the formation of free-bodies that can aggravate contact pressure inducing making it reach the yielding stress of the coatings and aggravating the wear process. A formation of an unstable trybolayer composed of oxides and free particles was also observed. This layer can lead do a decrease in wear coefficient since it's expected to present very high hardness as a result of plastic hardening.

5. References

[1] T. Liyanage, “Microstructure and Properties of Ni-Alloy and Ni-WC Composite Overlays,” University of Alberta, 2010.

[2] L. Venkatesh *et al.*, “Applied Surface Science Microstructure and phase evolution in laser clad chromium,” *Appl. Surf. Sci.*, vol. 357, pp. 2391–2401, 2015.

[3] M. J. Tobar, C. Álvarez, J. M. Amado, G. Rodríguez, and A. Yáñez, “Morphology and characterization of laser clad composite NiCrBSi-WC coatings on stainless steel,” *Surf. Coatings Technol.*, vol. 200, no. 22–23 SPEC. ISS., pp. 6313–6317, 2006.

[4] S. . Huang, M. Samandi, and M. Brandt, “Abrasive wear performance and microstructure of laser clad WC/Ni layers,” *Wear*, vol. 256, no. 11–12, pp. 1095–1105, 2004.

[5] J. Przybyøowicz and J. Kusin, “Structure of laser cladded tungsten carbide composite coatings,” *J. Mater. Process. Technol.*, vol. 109, no. 1–2, pp. 154–160, 2001.

[6] M. Erfanmanesh, R. Shoja-razavi, and H. Abdollah-pour, “Influence of using electroless Ni-P coated WC-Co powder on laser cladding of stainless steel,” *Surf. Coat. Technol.*, vol. 348, no. January, pp. 41–54, 2018.

[7] J. S. Xu, X. C. Zhang, F. Z. Xuan, Z. D. Wang, and S. T. Tu, “Microstructure and Sliding Wear Resistance of Laser Cladded WC / Ni Composite Coatings with Different Contents of WC Particle,” vol. 21, no. 9, pp. 1904–1911, 2012.

[8] K. Van Acker, D. Vanhoyweghen, R. Persoons, and J. Vangrunderbeek, “Influence of tungsten carbide particle size and distribution on the wear resistance of laser clad WC / Ni coatings,” *Wear*, vol. 258, no. 1–4, pp. 194–202, 2005.

[9] X. Tong, F. H. Li, M. Kuang, W. Y. Ma, X. C. Chen, and M. Liu, “Effects of WC particle size on the wear resistance of laser surface alloyed medium carbon steel,” *Appl. Surf. Sci.*, vol. 258, no. 7, pp. 3214–3220, 2012.

[10] R. Colaço and R. Vilar, “Abrasive wear of metallic matrix reinforced materials,” *Wear*, vol. 255, no. 1, pp. 643–650, 2003.

[11] C. Chan, J. Mazumder, and M. M. Chen, “A Two-Dimensional Transient Model for Convection in Laser Melted Pool,” *Metall. Trans. A*, vol. 15, no. 12, pp. 2175–2184, 1984.

[12] M. F. ASHBY and K. E. EASTERLING, “THE TRANSFORMATION HARDENING OF STEEL SURFACES BY LASER BEAMS-I . STEELS,” *Acta Met.*, vol. 32, no. 11, pp. 1935–1948, 1984.

[13] J. P. Angle, Z. Wang, C. Dames, and M. L. Mecartney, “Comparation of two-Phase Thermal conductivity Models with experiments on Dilute Ceramic Composites,” *J. Am. Ceram. Soc.*, vol. 96, no. 9, pp. 1–8, 2013.

[14] T. Nishi, H. Shibata, H. Ohta, and Y. Waseda, “Thermal Conductivities of Molten Iron , Cobalt , and Nickel by Laser Flash Method,” *Metall. Mater. Trans. A*, vol. 34, no. 12, pp. 2801–2807, 2003.

[15] A. C. G. Teixeira, “Caracterização de Propriedades Termo- Elétricas de Metal Duro,” 2016.

[16] Z. Turgut, M. Huang, K. Gallagher, and M. E. Mchenry, “Magnetic evidence for structural-phase transformations in Fe-Co alloy nanocrystals produced by a carbon arc Magnetic evidence for structural-phase transformations in Fe-Co alloy nanocrystals produced by a carbon arc,” *J. Appl. Phys.*, vol. 81, no. 8, pp. 4039–4041, 1997.

[17] I. Vernyhora, “Thermodynamics of fcc Ni – Fe Alloys in a Static Applied Magnetic Field,” *Thermodynamics*, no. February 2014, 2017.

[18] Y. Ustinovshikov, “A New Paradigm for Metallic Alloys in Materials Science,” *Adv. Mater. Phys. Chem.*, vol. 5, no. 1, pp. 244–270, 2015.

[19] K. Jin *et al.*, “Thermophysical properties of Ni-containing single-phase concentrated solid solution

alloys Thermophysical properties of Ni-containing single-phase concentrated solid solution alloys," *Mater. Des.*, vol. 117, no. 1, pp. 185–192, 2016.

[20] P. Kubicek and B. Vozniakova, "Study of tungsten in liquid iron diffusion coefficient dependency on temperature and concentration," *Radioisot. Appl. Metall.*, vol. 16, pp. 231–235, 1973.

[21] M. Walbrühl, A. Blomqvist, P. A. Korzhavyi, and C. M. Araujo, "Surface gradients in cemented carbides from first-principles-based multiscale modeling : Atomic diffusion in liquid Co," *J. Refract. Met. Hard Mater.*, vol. 66, no. 1, pp. 174–179, 2017.

[22] J. A. Kitchener and D. W. MORGAN, "Solutions in liquid iron," *Trans. Faraday Soc.*, vol. 67, no. 50, pp. 51–60, 1953.

[23] T. Saito, Y. Kawai, K. Maruya, and M. Maki, "Diffusion of Some Alloying Elements in Liquid Iron," *Sci. reports Res. Institutes, Tohoku Univ. Ser. A, Physics, Chem. Metall.*, vol. 11, pp. 401–410, 1959.

[24] D. Goldberg and G. R. Belton, "The Diffusion of Carbon in Iron-Carbon Alloys at 1560," *Metall. Trans.*, vol. 5, pp. 0–5, 1974.

[25] H. Qiyong, H. Tongfu, and W. Jian, "Determination of diffusion coefficient of carbon in liquid iron," *Acta Met. Sin*, vol. 16, pp. 435–441, 1980.

[26] E. Posner, "Mass transport and structural properties of liquid iron alloys at high pressure," 2017.

[27] A. Meyer, "The measurement of self-diffusion coefficients in liquid metals with quasielastic neutron scattering," vol. 01002, 2015.

[28] Q.-L. Cao and P.-P. Wang, "Stokes-Einstein relation in liquid iron-nickel alloy up to 300 GPa," *J. Geophys. Res. Solid Earth*, pp. 3351–3363, 2016.

[29] P. L. GRUZIN, "Certain laws of diffusion and distribution of elements in alloys," *METALLOVEDENIE*, no. 10, pp. 5–13, 1960.

[30] Q. Li, T. C. Lei, and W. Z. Chen, "Microstructural characterization of WCp reinforced Ni – Cr – B – Si – C composite coatings," *Surf. Coatings Technol.*, vol. 114, no. 1, pp. 285–291, 1999.

[31] K. Wieczerzak and G. Cios, "THE CHARACTERIZATION OF CAST Fe-Cr-C ALLOY," *Arch. Metall. Mater.*, vol. 60, no. 2, pp. 779–782, 2015.

[32] J. F. Shackelford, Y.-H. Han, S. Kim, and S.-H. Kwon, *Materials Science and Engineering Handbook*. 2015.

[33] AZoM, "Alumina - Aluminium Oxide - Al2O3 - A Refractory Ceramic Oxide," pp. 2–5, 2001.

[34] A. C. Fischer-cripps, "The Hertzian contact surface," *J. Mater. Sci.*, vol. 34, pp. 129–137, 1999.

[35] M. H. Staia *et al.*, "Cr2C3-NiCr VPS thermal spray coatings as candidate for chromium replacement To cite this version : HAL Id : hal-01070192 Science Arts & Métiers (SAM)," 2015.